Theor Chem Acc (2011) 129:31–43
DOI 10.1007/s00214-010-0882-8

REGULAR ARTICLE

# Modeling quantum vibrational excitations in condensed-phase molecular systems

**Andrea Amadei · Isabella Daidone · Laura Zanetti-Polzi · Massimiliano Aschi**

Received: 3 November 2010 / Accepted: 22 December 2010 / Published online: 13 January 2011


**Abstract** In this paper, we present an extension of the theoretical–computational methodology based on the perturbed matrix method and molecular dynamics simulations that we introduced in a recent paper (Daidone et al., Chem Phys Lett 488:213–218, 2010). This methodology models quantum vibrational states of polyatomic systems (i.e. beyond the one-dimensional vibrational mode case) embedded in a complex atomic-molecular environment such as liquid-state conditions. In the extended model, we now include the anharmonic correction to the excitation frequency of each mode and the excitonic coupling effects, providing a detailed description of the theoretical basis and an explicit scheme to achieve a very efficient implementation of the method. Application of the proposed procedure to study the amide I band of the infrared spectra of a $\beta$-hairpin peptide shows that a quantitative and accurate reproduction of the experimental spectral variations due to folding–unfolding transition can be achieved.

**Keywords** Infrared spectroscopy · Protein folding · Molecular dynamics simulation · Quantum chemistry

A. Amadei (✉)
Dipartimento di Scienze e Tecnologie Chimiche,
University of Rome "Tor Vergata", via della Ricerca
Scientifia 1, 00133 Rome, Italy
e-mail: andrea.amadei@uniroma2.it

I. Daidone · M. Aschi
Dipartimento di Chimica Ingegneria Chimica e Materiali,
University of L'Aquila, via Vetoio (Coppito 1),
67010 Coppito, AQ, Italy

L. Zanetti-Polzi
Dipartimento di Chimica, University of Rome "La Sapienza",
P.le Aldo Moro 5, 00185 Rome, Italy

## 1 Introduction

Theoretical modeling of infrared (IR) spectra of polyatomic molecules in condensed phase is one of the most challenging lines of research in theoretical physical chemistry. Beyond its intrinsically interesting aspects, a correct modeling of IR spectroscopic signals might be of great practical importance since such a technique is among the most utilized to address several relevant problems, in particular in the biochemical field. For example, by means of time-resolved [1] and bidimensional [2] IR spectroscopy, it is possible to characterize ligand migration in proteins [3, 4] and folding/unfolding kinetics in peptides [5–11]. The complexity of the spectroscopic signal, as emerging from the structural fluctuations of the polypeptide chain and from its interaction with the solvent, makes it difficult, though, to properly interpret the spectra in terms of structural features and transitions of the solvated peptide or protein. Theoretical–computational methods may thus provide essential information on the complex absorption–structure relation, shedding light on the IR spectroscopic effects of structural transitions, the polypeptide sequence, and the interaction with the solvent.

The IR spectroscopic behavior of small solvated molecules, such as trans-N-methylacetamide (trans-NMA) [12], a model system of the peptide group, or a tri-alanine peptide [13], has been successfully described by means of several strategies either based on an entirely classical view of the system, i.e. using the electric dipole auto-correlation function along classical molecular dynamics (MD) trajectories [12–16], or based on a fully quantum description of the chromophore at expenses of the classical sampling [17]. Alternative methods [18–20] combining electronic structure/molecular dynamics calculations make use of an empirical relation providing the instantaneous frequency of

a solute as obtained by fitting *ab initio* vibrational frequencies of a solute–solvent cluster either to a linear combination of the electrostatic potentials [19] or to the components of the electric fields [18, 20] acting on the solute atoms.

For the study of peptides and small proteins, and more in general molecules in solution, other methods have appeared in the literature [15, 21–31]. Many of these [15, 22, 23, 27–37] employ quantum mechanical (QM) calculations to determine the vibrational frequencies and eigenstates for single amides which are then transferred to the full peptides and/or proteins and coupled empirically (see below). With an alternative approach [24–26], Hessian calculations on the entire isolated peptide/protein in a given configuration can be used to reconstruct the local, single-residue, vibrational frequencies via the Hessian matrix reconstruction method [26]. In these approaches, coupling effects are included by adding a simplified electrostatic interaction, typically based on dipole–dipole interactions and commonly termed transition dipole coupling—TDC (coupling through space) and an empirical term providing the frequency variations due to first-neighbors relative rotations (coupling through chemical bonds). The solvatochromic effect, when included, is modeled via an empirical term relating the single-residue frequency to the perturbing electric potential exerted by the solvent, as obtained by calculations on solute/solvent clusters and MD simulation.

A number of these studies [15, 22–24, 27, 29, 31, 38, 39] have suggested that the amide I absorption patterns of folded structural elements, such as the $\beta$-sheet, can be explained by the symmetry of the given structure and point to a crucial role played by excitonic coupling of the amide I oscillators. On the contrary, the physical origin of the spectroscopic behaviors of unfolded states is much less understood, although the differences in the amide I bands of folded and unfolded states have become a crucial spectral feature to follow protein- and peptide-folding kinetics in time-resolved and temperature-dependent IR spectroscopies [6, 7, 9–11].

In this context, we have lately presented a theoretical–computational approach to calculate IR spectra in condensed phase [21, 40, 41] based on MD simulations and on the perturbed matrix method [42–45] (PMM), whose philosophy is to keep the configurational complexity of the system with a proper treatment of the quantum degrees of freedom of the chemical system treated at quantum mechanical level, the quantum center (QC). Within this basic approximation, this method was successfully applied to reproduce the IR spectrum of carbon monoxide in aqueous solution [40] and within myoglobin [46], as well as, more recently, to describe the IR signal of two different $\beta$-hairpin peptides [41].

The main aim of our methodology is to provide a general, rigorous procedure, based on physical derivations without involving phenomenological parameters, able to reproduce the essential physics underlying IR excitations of complex molecular systems, also in the case of a chromophore exhibiting a high structural flexibility (e.g. peptides' and proteins' unfolded states). In the PMM procedure, the coupling between the quantum states of the QC and its atomic-molecular environment, providing the inhomogeneous broadening and hence essential to reproduce the spectral signal, is modeled by considering the quantum center as embedded into the perturbing electric field exerted by the QC environment. Therefore, the effects of the perturbing field on the QC quantum states (corresponding to the QC–environment coupling) can be obtained via first principles derivations providing at each MD frame the corresponding perturbed vibrational states and frequencies. The explicit modeling of the perturbation operator via the perturbing electric field has been also exploited by Mukamel and coworkers, who have proposed in the last years a method for the calculation of IR spectra [47, 48] bearing similarities with our PMM/MD approach. In their method, the effect of the perturbing electric field is introduced as a perturbation of the QC vibrational energy surface neglecting any perturbation of the electronic (ground) state, thus essentially corresponding to a first-order perturbation theory approach. In our PMM/MD procedure, we explicitly model, by means of the perturbing electric field and high level electronic structure calculations, the electronic Hamiltonian operator providing the QC perturbed electronic states and energies and hence allowing the direct calculation of the perturbed vibrational energy along the mode coordinates considered.

In the present study, we extend this approach by including the anharmonic effects of each vibrational mode and the excitonic coupling, both disregarded in previous papers. In the Sect. 2, along with the new extension, we thoroughly describe the essential features of the general theoretical approach previously reported [40], specifically deepening some key basic points involved in modeling vibrational quantum states of rotating systems and treating a polyatomic QC, i.e. the multidimensional vibrational modes case, introducing in the model a correction for (moderate) anharmonic vibrational behavior and the excitonic coupling. Finally, in the Sect. 4, we apply the PMM/MD-based procedure to reproduce the IR amide I band of trans-NMA and of the $\beta$-hairpin peptide previously studied with the simpler procedure [21, 41], comparing our results with the experimental spectra.

## 2 Theory

The theoretical framework described in the Sect. 2 represents an extension of the model presented in previous

papers [40, 41] concerning the use of perturbed Born–Oppenheimer (BO) surfaces, corresponding to different electronic eigenstates, to obtain an accurate description of molecular vibrational states via PMM calculations. In the first and second subsections, the harmonic model and its anharmonic extension are presented. Finally, in the last subsections, we illustrate how to construct in practice the theoretical model for the perturbed vibrational states, via an efficient implementation based on a simple approximation, and provide an explicit model to treat excitonic coupling. In Appendix 1, we provide a schematic description of the computational methodology employed, summarizing all the relevant steps in the procedure.

### 2.1 The harmonic model

Let us consider a system defined by a semiclassical atomic-molecular environment, e.g. the solvent molecules, surrounding a rigid molecule or chemical group (the previously defined QC) with semiclassical rototranslational degrees of freedom, i.e. the Cartesian internal coordinates are quantum vibrational degrees of freedom and the mass tensor is a block diagonal matrix with the internal coordinates block decoupled from the rototranslational one [49, 50]. Within such a definition of the QC and its perturbing semiclassical environment, we may obtain the QC (harmonic) vibrational states associated with the perturbed electronic ground state via [40]

$$\hat{H}_v \phi_v \cong \mathcal{U}_v \phi_v \tag{1}$$

$$\hat{H}_v = \hat{K}_\beta + \Delta\boldsymbol{\beta}^T \frac{\widetilde{A}}{2} \Delta\boldsymbol{\beta} \tag{2}$$

$$\hat{K}_\beta = \hat{\boldsymbol{\pi}}_\beta^T \frac{\widetilde{D}_{\beta,\beta}}{2} \hat{\boldsymbol{\pi}}_\beta \tag{3}$$

where $\boldsymbol{\beta}$ are the Cartesian internal coordinates, $\hat{H}_v$ is the vibrational Hamiltonian operator defined by the kinetic energy $\hat{K}_\beta$ and potential energy $\Delta\boldsymbol{\beta}^T \frac{\tilde{A}}{2} \Delta\boldsymbol{\beta}$ operators, $\hat{\boldsymbol{\pi}}_\beta$ are the $\boldsymbol{\beta}$ conjugated momenta operators, $\widetilde{D}_{\beta,\beta}$ is the inverse mass tensor (diagonal) block corresponding to the internal coordinates (i.e. the inverse of the internal coordinates mass tensor block) and $\widetilde{A}$ is the Hessian matrix in $\boldsymbol{\beta}$ for the electronic ground-state energy as obtained in the electronic energy minimum at $\boldsymbol{\beta} = \boldsymbol{\beta}_0$ for a given environment and QC rototranslational configuration. Note that our definition of the conjugated momenta operators, as described in details in our previous paper [40], is fully consistent with the classical mechanical conjugated momenta definition but it does not necessarily ensure reality of the operators [51], i.e. Hermiticity of the corresponding matrix. For such a reason the $\hat{\boldsymbol{\pi}}$ operators as defined here, although widely used, are not always considered as the "true" conjugated momenta operators. For sake of simplicity in this paper, as in our previous paper, we refer to $\hat{\boldsymbol{\pi}}$ as the conjugated momenta operators, hence focusing on the correspondence and reproduction of the classical mechanical definition and relations. Finally, $\phi_v$ is the vibrational wave function, $\mathcal{U}_v$ the corresponding (vibrational) energy and $\Delta\boldsymbol{\beta} = \boldsymbol{\beta} - \boldsymbol{\beta}_0$.

It is convenient to express the Hamiltonian operator $\hat{H}_v$ via the mass-weighted coordinates ($\boldsymbol{\xi} = \sqrt{\widetilde{D}_{\beta,\beta}^{-1}}\,\boldsymbol{\beta}$) and corresponding conjugated momenta ($\boldsymbol{\pi}_\xi = \sqrt{\widetilde{D}_{\beta,\beta}}\,\boldsymbol{\pi}_\beta$)

$$\hat{H}_v = \frac{\hat{\boldsymbol{\pi}}_\xi^T \hat{\boldsymbol{\pi}}_\xi}{2} + \Delta\boldsymbol{\xi}^T \sqrt{\widetilde{D}_{\beta,\beta}} \frac{\tilde{A}}{2} \sqrt{\widetilde{D}_{\beta,\beta}} \Delta\boldsymbol{\xi} \tag{4}$$

which may be simplified by using the orthogonal transformation (in mass-weighted space) $\boldsymbol{\xi}, \boldsymbol{\pi}_\xi \rightarrow \boldsymbol{q}, \boldsymbol{\pi}_q$ diagonalizing the mass-weighted Hessian $\sqrt{\widetilde{D}_{\beta,\beta}}\,\tilde{A}\,\sqrt{\widetilde{D}_{\beta,\beta}}$

$$\hat{H}_v = \sum_j \hat{H}_{v,j} \tag{5}$$

$$\hat{H}_{v,j} = \frac{1}{2}\left[ (\hat{\boldsymbol{\pi}}_q^T)_j \hat{\pi}_{q_j} + \Delta q_j \omega_j^2 \Delta q_j \right] \tag{6}$$

where $j$ runs over the internal coordinates' modes defined by the mass-weighted Hessian eigenvectors, $\omega_j^2$ are the corresponding eigenvalues providing the modes frequencies and from the definition of the conjugated momenta operators [40] (see Appendix 2)

$$\hat{\pi}_{q_j} = -i\hbar \frac{\partial}{\partial q_j} \tag{7}$$

$$(\hat{\boldsymbol{\pi}}_q^T)_j = -i\hbar \sum_{j'} \frac{\partial(\partial r_{n,j'}/\partial q_j)}{\partial r_{n,j'}} + \hat{\pi}_{q_j} \tag{8}$$

with $j'$ running over all the nuclear Cartesian coordinates $\boldsymbol{r}_n$ of the QC, as expressed in the laboratory fixed frame. From the last equations, we readily obtain that the QC vibrational wave function may be considered as the product of the modes wave functions, i.e. $\phi_v(\boldsymbol{q}) = \Pi_j \phi_{v,j}(q_j)$ where, for each $j$th mode, we may obtain the vibrational states/wave functions and relative energies via

$$\hat{H}_{v,j}\phi_{v,j,m} = -\frac{\hbar^2}{2}\left( \sum_{j'} \frac{\partial(\partial r_{n,j'}/\partial q_j)}{\partial r_{n,j'}} \right) \frac{\partial \phi_{v,j,m}}{\partial q_j} - \frac{\hbar^2}{2} \frac{\partial^2 \phi_{v,j,m}}{\partial q_j^2} + \frac{\omega_j^2}{2} \Delta q_j^2 \phi_{v,j,m} \cong \mathcal{U}_{v,j,m} \phi_{v,j,m} \tag{9}$$

with $m$ expressing the vibrational state of the $j$th mode.

It is worth to note that being the $\boldsymbol{q}$ coordinates a linear transformation of the QC internal Cartesian coordinates, the nuclear Cartesian coordinates in the laboratory fixed frame $\boldsymbol{r}_n$ are linearly dependent on $\boldsymbol{q}$ and hence $(\partial r_{n,j'}/\partial q_j)$ is a function only of the Eulerian angles describing the rotational position of the QC frame with respect to the

laboratory fixed frame [49, 50] ($\boldsymbol{r}_n$ are also linearly dependent on the center of mass position providing the QC translational coordinates). Therefore, for a rotationally constrained QC, we have $\frac{\partial(\partial r_{n,j'}/\partial q_j)}{\partial r_{n,j'}} = 0$ and hence in such a case Eq. 9 would reduce to the usual equation for the vibrational states of a harmonic coordinate (note that for the isolated QC, the vibrational modes and frequencies as obtained by the internal Cartesian coordinates mass-weighted Hessian coincide with those obtained by the whole $\boldsymbol{r}_n$ mass-weighted Hessian as it follows from the fact that the former is the non-singular minor of the latter).

Equation 9 clearly shows that even for a rigid QC, where from a classical point of view rototranslational and internal motions are fully decoupled, different vibrational eigenstates are in principle obtained for rotationally constrained and unconstrained QCs. Such a remarkable result, illustrating a peculiar quantum mechanical coupling between rotations and internal vibrations, is typically neglected when dealing with a rigid QC with classical rotational motions (the case considered in this paper) as for such a condition uncoupled rotational and internal motions are to be expected. Note that in the limit of a huge spatial distribution of QC atomic masses, ensuring purely classical rotations, we always have $\frac{\partial(\partial r_{n,j'}/\partial q_j)}{\partial r_{n,j'}} \cong 0$ as it follows from the fact that in such a case the variation of a single atomic coordinate would virtually leave unaltered the Eulerian angles. In practice, a combination of partly constrained rotations (as provided by high-energy interactions in condensed phase) and a reasonably extended atomic mass spatial distribution makes it possible to use of the simple harmonic coordinate equation

$$\begin{aligned}\hat{H}_{v,j}\phi_{v,j,m} &\cong -\frac{\hbar^2\partial^2\phi_{v,j,m}}{2\ \partial {q_j}^2} + \frac{\omega_j^2}{2}\Delta q_j^2\phi_{v,j,m} \\ &\cong \mathcal{U}_{v,j,m}\phi_{v,j,m}\end{aligned} \tag{10}$$

providing the (standard) vibrational eigenstates of the $j$th mode. Whether such an approximation is always accurate and which limitations are to be considered, although representing an interesting theoretical problem, is beyond the scope of the present work, and hence, it will not be addressed in this paper.

## 2.2 The anharmonic correction

In the previous subsection, we have assumed that the (ground-state) electronic energy surface in the internal nuclear degrees of freedom may be well described by a quadratic function of such coordinates. This approximation, typically rather accurate when we deal, as in the present paper, with the first vibrational excited states only, may however be improved by considering the weak anharmonic perturbation affecting the first vibrational excitations.

Many theoretical–computational procedures have been proposed in the last years for properly addressing anharmonicity [52–59]. In the present case, we assume that such anharmonic effects are so weak that we may still use the Hessian eigenvectors to decompose the vibrational Hamiltonian operator, hence providing a set of independent Hamiltonian equations for each mode (similarly to Eq. 10) with however the potential energy operator given by a function beyond the quadratic form. Such an approximation, disregarding the anharmonic effects due to modes coupling, allows a simple and efficient implementation, and it is likely to provide a relevant part of the anharmonic correction to be used for the first vibrational excitations. More complex corrections [60], although possible, require the use of computationally demanding perturbative approaches, necessarily leading to inefficient implementations to treat liquid-state systems.

A simple, physically reasonable potential energy function beyond the quadratic approximation, providing an analytical solution to the jth mode Hamiltonian equation, is the Morse potential [61]

$$\mathcal{U}_{M,j}(q) = V_{0,j} + \delta_j\left[1 - e^{-\frac{\omega_j(q_j - q_{0,j})}{\sqrt{2\delta_j}}}\right]^2 \tag{11}$$

then leading to

$$\hat{H}_{v,j}\phi_{v,j,m} \cong -\frac{\hbar^2\partial^2\phi_{v,j,m}}{2\ \partial {q_j}^2} + \mathcal{U}_{M,j}(q)\phi_{v,j,m} \cong \mathcal{U}_{v,j,m}\phi_{v,j,m} \tag{12}$$

with $q_{0,j}$ and $V_{0,j}$ the minimum energy position and corresponding energy, respectively, $\delta_j$ a parameter defining the energy variation in the $q \to \infty$ limit and, clearly, $\omega_j$ the harmonic pulsation (i.e. the harmonic frequency multiplied by 2 $\pi$) as obtained by the mass-weighted Hessian eigenvalue. Solution of the last equation provides [61]

$$\begin{aligned}\mathcal{U}_{v,j,m+1} - \mathcal{U}_{v,j,m} &= \hbar\omega_j - \frac{\hbar^2\omega_j^2}{4\delta_j}\left[1 + 2\left(m + \frac{1}{2}\right)\right] \\ &= \hbar\omega_j - \frac{\hbar^2\gamma_j^2}{18\omega_j^4}\left[1 + 2\left(m + \frac{1}{2}\right)\right]\end{aligned} \tag{13}$$

where $\gamma_j$ is the third-order derivative of $\mathcal{U}_{M,j}$ as obtained at the minimum position $q_{0,j}$. It is worth to note that in usual conditions (weak anharmonic perturbation), the vibrational wave functions for the ground and first excited states, as provided by Eq. 12, are virtually indistinguishable from the corresponding harmonic solutions and, hence, except for the energy for which the anharmonic correction given in Eq. 13 is necessary, all the other properties may be typically well approximated by the corresponding harmonic

ones (i.e., they can be obtained by using the harmonic wave functions).

### 2.3 The invariant mode approximation

From the results of the previous subsections, it is clear that we have to evaluate, via PMM, the QC perturbed mass-weighted Hessian at each QC–environment configuration to obtain the proper modes and frequencies by the Hessian diagonalization and the corresponding anharmonic correction. In practice, such a procedure, although in principle possible, is highly computationally expensive when a polyatomic QC in liquid-state conditions is considered and hence a simplification is necessary in order to keep a proper statistical sampling (i.e. calculations over a huge phase space sampling) ensuring meaningful vibrational properties.

A reasonable and typically accurate approximation can be achieved assuming that for the modes of interest, the perturbation may provide QC modes coupling effects only within a limited dimensional subspace, hence requiring the calculation of the perturbed Hessian only for the corresponding low dimensional subspace. In particular, when it is reasonable to assume, as in the present paper, that such a subspace reduces to a single quantum vibrational degree of freedom, i.e. the environment perturbation does not significantly alter the vibrational modes (the mass-weighted Hessian eigenvectors) but only induces relevant variations of the corresponding frequencies, we obtain the most efficient simplification. It must be remarked that such an approximation is valid as far as the concerned vibrational modes can be considered as "local" uncoupled modes essentially independent of the other vibrational modes, i.e. they can be properly defined by the Hessian of the isolated QC. For such type of vibrational modes, once the unperturbed mass-weighted Hessian eigenvectors are defined by a preliminary calculation, we may obtain the $\omega_j^2$ value and the anharmonic correction (see Eq. 13) at each QC–environment configuration via a polynomial fit to the perturbed electronic ground-state energy along the corresponding $j$th mode (unperturbed eigenvector), with the same procedure used for a simple bi-atomic molecule [40]. Therefore, a straightforward PMM application along each vibrational mode of interest, providing the corresponding perturbed electronic ground-state energy curve, ensures a computationally efficient evaluation of the (quantum) vibrational behavior of a polyatomic system.

In practice, once defined with $\mathcal{V}$ and $\boldsymbol{E}$ the perturbing electric potential and field exerted by a classical molecular environment on the quantum center (typically obtained by the environment atomic charge distribution) and with $\widetilde{H}^0$ and $\widetilde{H}$ the unperturbed and perturbed (electronic) Hamiltonian matrices of the QC, we can obtain the perturbed electronic eigenstates and eigenenergies of the quantum center diagonalizing the perturbed Hamiltonian matrix given by [40, 42, 44, 45]

$$\widetilde{H} \cong \widetilde{H}^0 + \widetilde{I} q_T \mathcal{V} + \widetilde{Z}_1 + \Delta V \widetilde{I} \tag{14}$$

$$\left[\widetilde{Z}_1\right]_{k,k'} = -\boldsymbol{E} \cdot \langle \Phi_k^0 | \hat{\boldsymbol{\mu}} | \Phi_{k'}^0 \rangle \tag{15}$$

where $q_T$ is the total charge of the QC, $\hat{\boldsymbol{\mu}}$ and $\Phi_k^0$ are the dipole operator and unperturbed electronic eigenfunction of the QC, $\Delta V$ approximates all the higher-order terms as a simple short range potential and the angled brackets mean integration over the electronic coordinates ($\widetilde{I}$ is the identity matrix). Note that $\widetilde{H}$ can be evaluated for each QC and environment configuration, and hence its eigenvectors and eigenvalues describe all the possible electronic states and energies along the chosen vibrational mode within a given statistical ensemble as provided by the MD simulation. The perturbed electronic ground-state energy, (i.e. the ground-state eigenvalue of the matrix $\widetilde{H}$), along the mode coordinate can then provide the perturbed frequency at each time frame [41] via estimating the second and third order energy derivatives at the minimum position (i.e. $\omega_j^2$ and $\gamma_j$, respectively) which are used to obtain the harmonic frequency ($\omega_j/2\pi$) and the anharmonic correction (see Eq. 13). In case of a single vibrational center or a multi-chromophore system where we may disregard excitonic coupling, the obtained perturbed frequencies and vibrational states may be used to obtain the IR spectrum which then may be considered as given by the superposition of the excitations of localized perturbed vibrational modes.

The IR spectral signal of a chromophore mode, for unitary radiation energy density per unit frequency, can be obtained via the corresponding absorption coefficient for the $0 \rightarrow 1$ vibrational transition (higher excitations may be considered as essentially forbidden), which can be expressed by

$$\varepsilon_{0,1}(\nu) = \frac{|\boldsymbol{\mu}_{0,1}|^2 \rho(\nu) h\nu}{6\epsilon_0 c \hbar^2} \tag{16}$$

where $\rho(\nu)$ is the probability density in the excitation frequency space $\nu$, $\varepsilon_0$ is the vacuum dielectric constant, $c$ is the (vacuum) light speed and, making use of the linear approximation for the (perturbed) electronic ground-state dipole $\boldsymbol{\mu}_0^e(q) \cong \boldsymbol{\mu}_0^e(q_0) + \boldsymbol{\eta}_0(q - q_0)$, the (perturbed) transition dipole $\boldsymbol{\mu}_{0,1}$ may be expressed by

$$\begin{aligned} \boldsymbol{\mu}_{0,1} &= \langle \phi_{v,0} | \boldsymbol{\mu}_0^e(q) | \phi_{v,1} \rangle \cong \boldsymbol{\eta}_0 \langle \phi_{v,0} | q - q_0 | \phi_{v,1} \rangle \\ &\cong \boldsymbol{\eta}_0^0 \sqrt{\frac{\hbar^2}{2\hbar\omega}} \end{aligned} \tag{17}$$

with $\boldsymbol{\eta}_0^0$ the unperturbed (gas phase) electronic ground-state dipole derivative in the mode coordinate $q$, which for most of the molecular systems of interest is virtually identical to

the perturbed value, i.e. $\boldsymbol{\eta}_0^0 \cong \boldsymbol{\eta}_0$, thus allowing a considerable reduction of the computational costs. It must be remarked that in the last equation we made use of $\langle \phi_{v,0}|q-q_0|\phi_{v,1}\rangle \cong \sqrt{\frac{\hbar^2}{2\hbar\omega}}$ due to approximating the solutions of Eq. 12 with the corresponding harmonic wave functions (given by Eq. 10) for the calculation of all the vibrational properties except, of course, the energy given by Eq. 13. As mentioned in the previous subsection, such an approximation, we will use throughout this paper, is accurate when we consider weakly anharmonic effects as typically occurs for the vibrational ground and first excited states. Finally, the IR signal of a molecule involving several vibrational centers can be obtained by summing the absorption coefficients of all the chromophores modes of interest, hence reconstructing the complete spectral signal [41]. It is worth to note that in these last equations, besides neglecting of the possible excitonic coupling treated in the following subsection, we actually disregard higher order effects such as the homogeneous broadening (arising from the finite lifetime of the excited state), the Doppler effect and motional narrowing. However, such further spectral terms, although may be in principle treated explicitly, provide only slight effects which are typically below the computational resolution achieved (0.5–1 $\mathrm{cm}^{-1}$) and hence are omitted in our calculations.

### 2.4 The excitonic coupling

When modes coupling effects due to interacting vibrational centers (chromophores) cannot be neglected, excitonic effects ought to be considered. Following the procedure described in details in a recent paper addressing the excitonic coupling of electronic states [43], here we extend the method to model the excitonic coupling of vibro-electronic (vibronic) states. The basis set obtained via the solution of Eq. 12 for the modes of each vibrational center of interest may be used to construct the complete excitonic Hamiltonian matrix of the interacting chromophores. Diagonalization of this matrix provides the (delocalized) vibrational states of the excitonic system, hence including in the model higher-order anharmonic effects.

The reference basis set to be used in constructing the excitonic vibronic Hamiltonian matrix is here defined by considering a single excited chromophore in each reference excited state (single-photon excitations). This provides at a given classical configuration, for the reference (excited) state characterized by the *kth* chromophore with the *nth* mode of the *pth* electronic state in the *mth* vibrational state, the wave function $\Psi^{ref}_{k,n,p,m} = \chi^{n,m}_{k,p}\Pi_{l\neq k}\chi_{l,0}$ where the *lth* chromophore (perturbed) vibronic ground state $\chi_{l,0}$ and the *kth* chromophore (perturbed) vibronic excited state $\chi^{n,m}_{k,p}$ (with $p+m \geq 1$) are given by

$$\chi_{l,0} = \Phi_{l,0}\Pi_j \phi_{v,l,j,0,0} \tag{18}$$

$$\chi^{n,m}_{k,p} = \Phi_{k,p}\phi_{v,k,n,p,m}\Pi_{j\neq n}\phi_{v,k,j,p,0} \tag{19}$$

In the last equations, $l$ runs over the chromophores, $j$ runs over the modes, $\Phi_{l,0}, \Phi_{k,p}$ are the (perturbed) electronic ground and *pth* state of the *lth* and *kth* chromophore, respectively, as obtained by PMM electronic-state calculations, $\phi_{v,l,j,0,0}$ is the (perturbed) *jth* mode vibrational ground state of the *lth* chromophore electronic ground state and $\phi_{v,k,n,p,m}$ is the (perturbed) *nth* mode vibrational *mth* state of the *kth* chromophore electronic *pth* state, both obtained by solving Eq. 12. Finally, within the same notation, the reference ground state is then given by $\Psi^{ref}_0 = \Pi_l \chi_{l,0}$, where within the approximations used, $\Psi^{ref}_0 = \Psi_0$ (i.e. the vibronic ground state is identical to the reference vibronic ground state).

We can obtain the excitonic states and excitation energies by diagonalization of the excitonic Hamiltonian matrix (i.e. the Hamiltonian matrix for the interacting chromophores) given by [43]

$$\widetilde{H} = \widetilde{I}\mathcal{U}_{vb,0} + \Delta\widetilde{H} \tag{20}$$

with $\mathcal{U}_{vb,0}$ the (vibronic) ground-state energy of the interacting chromophores and $\Delta\widetilde{H}$ the excitation matrix whose non-zero elements (in atomic units) are

$$\left[\Delta\widetilde{H}\right]_{\Psi^{ref}_{k,n,p,m},\Psi^{ref}_{k,n,p,m}} = \mathcal{U}^{n,m}_{vb,k,p} - \mathcal{U}_{vb,k,0} \tag{21}$$

$$\left[\Delta\widetilde{H}\right]_{\Psi^{ref}_{k,n,p,m},\Psi^{ref}_{k',n',p',m'}} = \frac{\langle\chi^{n,m}_{k,p}|\hat{\boldsymbol{\mu}}_k|\chi_{k,0}\rangle\cdot\langle\chi_{k',0}|\hat{\boldsymbol{\mu}}_{k'}|\chi^{n',m'}_{k',p'}\rangle}{R^3_{k,k'}} - 3\frac{\langle\chi_{k',0}|\hat{\boldsymbol{\mu}}_{k'}|\chi^{n',m'}_{k',p'}\rangle\cdot\boldsymbol{R}_{k,k'}\langle\chi^{n,m}_{k,p}|\hat{\boldsymbol{\mu}}_k|\chi_{k,0}\rangle\cdot\boldsymbol{R}_{k,k'}}{R^5_{k,k'}} \tag{22}$$

where $k \neq k', \boldsymbol{R}_{k,k'}$ is the $k'$ to $k$ chromophore displacement vector defined by the corresponding chromophores' origins (typically the centers of mass), $\hat{\boldsymbol{\mu}}_l$ is the *lth* chromophore dipole operator, $\mathcal{U}^{n,m}_{vb,k,p}$ is the (perturbed) vibronic energy of the *kth* chromophore in the *pth* electronic state with the *nth* mode in the *mth* vibrational state and $\mathcal{U}_{vb,k,0}$ the (perturbed) vibronic ground-state energy of the *kth* chromophore, both obtained by PMM calculations. Following our previous paper [43], we may also obtain the transition dipole for the excitation to the *ith* excitonic state ($\boldsymbol{\mu}_{0,i}$ with $i \geq 1$) via

$$\boldsymbol{\mu}_{0,i} = \sum_{k,n,p,m} c_{i,k,n,p,m}\langle\chi_{k,0}|\hat{\boldsymbol{\mu}}_k|\chi^{n,m}_{k,p}\rangle \tag{23}$$

$$c_{i,k,n,p,m} = \langle\Psi_i|\Psi^{ref}_{k,n,p,m}\rangle \tag{24}$$

with, clearly, $c_{i,k,n,p,m}$ the $\Psi^{ref}_{k,n,p,m}$ component of the *ith* excitonic state, i.e. the *ith* eigenvector of $\Delta\widetilde{H}$ (note that $c_{i,k,n,0,0} = 0$ for any excitonic state with $i \geq 1$).

When we deal with the excitonic coupling of vibrational states only (as in the present applications), the previous equations are simplified by considering that for each chromophore only the first vibrational excitation of the electronic ground state must be involved, as higher vibrational excitations are forbidden and the coupling with excited electronic states may be neglected. Therefore, by using the derivations and approximations described in the previous subsections, we have that the only non-zero elements of the relevant diagonal block of the excitation matrix are

$$\left[\Delta\widetilde{H}\right]_{\Psi^{ref}_{k,n,0,1},\Psi^{ref}_{k,n,0,1}} = \mathcal{U}^{n,1}_{vb,k,0} - \mathcal{U}_{vb,k,0} = h\nu_k \tag{25}$$

$$\left[\Delta\widetilde{H}\right]_{\Psi^{ref}_{k,n,0,1},\Psi^{ref}_{k',n',0,1}} \cong \sqrt{\frac{\hbar^2}{2\hbar\omega_{k,n}}}\sqrt{\frac{\hbar^2}{2\hbar\omega_{k',n'}}}\,\frac{\boldsymbol{\eta}^0_{k,n,0}\cdot\boldsymbol{\eta}^0_{k',n',0}}{R^3_{k,k'}} - 3\sqrt{\frac{\hbar^2}{2\hbar\omega_{k,n}}}\sqrt{\frac{\hbar^2}{2\hbar\omega_{k',n'}}}\,\frac{\boldsymbol{\eta}^0_{k',n',0}\cdot\boldsymbol{R}_{k,k'}\boldsymbol{\eta}^0_{k,n,0}\cdot\boldsymbol{R}_{k,k'}}{R^5_{k,k'}} \tag{26}$$

and the transition dipole for the $0 \rightarrow i$ excitonic transition is

$$\mu_{0,i} \cong \sum_{k,n} c_{i,k,n,0,1}\sqrt{\frac{\hbar^2}{2\hbar\omega_{k,n}}}\boldsymbol{\eta}^0_{k,n,0} \tag{27}$$

Note that in the last equations $\nu_k$ is the *kth* chromophore vibrational excitation frequency and in the summation of Eq. 27, we removed the electronic and vibrational state indexes $p$ and $m$ (see E. 23) as in the reference basis set we now involve the vibronic ground state and first vibrational excitations only. Finally, we may reconstruct the spectral signal of the excitonic system by summing the absorbance due to each $0 \rightarrow i$ transition, providing

$$\varepsilon(\nu) = \sum_i \frac{|\boldsymbol{\mu}_{0,i}|^2\rho_i(\nu)h\nu}{6\epsilon_0 c\hbar^2} \tag{28}$$

with $\rho_i$ the probability density in frequency space for the *ith* excitation.

## 3 Computation details

### 3.1 Trans-NMA

Quantum chemical calculations were carried out on the isolated trans-NMA molecule at the time-dependent density functional theory (TD-DFT) level with the 6-31+G(d) basis set. This level of theory was selected because it represents a good compromise between computational costs and accuracy. The mass-weighted Hessian matrix was calculated on the optimized geometry at the B3LYP/6-31+G(d) level of theory and subsequently diagonalized to obtain the unperturbed eigenvectors and related eigenvalues. The eigenvector corresponding in vacuo to the amide I mode was then used to generate a grid of points (i.e. configurations) as follows: a step of 0.05 a.u. was adopted, and the number of points was set to span an energy range of 20 kJ/mol (in the present case 31 points). For each point, six unperturbed electronic states were then evaluated at the same level of theory providing the basis set for PMM electronic calculations, i.e. the $\Phi^0$ eigenfunctions. All the unperturbed QM calculations were performed using the Gaussian03 package [62].

A 20-ns-long atomistic MD simulation of trans-NMA in aqueous solution was performed in explicit solvent by using the program GROMACS [63] and the GROMOS96 force field [64]. For the trans-NMA, the DFT-based optimization described above was used and the atomic charges were calculated using standard fitting procedures [65] on the optimized geometry at the B3LYP/6-31+G(d) level of theory. The solvent used was $D_2O$, to reproduce the experimental conditions, and was modeled using the deuterated SPC water model [66] at a density of 55.32 mol/l. Both bond lengths and the overall rototranslational degrees of freedom were constrained [49, 67]. Periodic boundary conditions were used, and the long-range electrostatic interactions were treated with the particle mesh Ewald method [68]. Coordinates were saved every ps. Simulations were performed in the NVT ensemble with the isokinetic temperature coupling [69] to keep the temperature constant at 300 K.

### 3.2 GS10 peptide

The Gramicidin S analog GS10 is a $\beta$-hairpin peptide whose primary structure is: cyclo[(Val-Lys-Leu-Tyr-Pro)$_2$]. Two 300-ns-long atomistic MD simulation of GS10 at different temperatures (280 K, 360 K) were performed in explicit solvent. The initial structures, representing the folded state, were taken from a simulation of 10 ns that was started from a structure generated on the basis of the experimental chemical structure [70].

The solvent used was $D_2O$, to reproduce the experimental conditions, and was modeled using the deuterated SPC water model [71]. Both starting configurations were placed in a cubic water box large enough to contain the peptide and at least 1.0 nm of solvent on all sides at a water density of 55.32 mol/l. Two negative ($Cl^-$) counterions were added by replacing the corresponding number of water molecules so as to achieve a neutral simulation box. The MD simulation protocol was the same as described for trans-NMA.

The simulations at 280 K and 360 K were used to obtain the spectroscopic signal to be compared to the experimental data available in literature.

## 4 Results and discussion

### 4.1 Infrared spectrum in the amide I region of aqueous trans-NMA

The amide I band of the aqueous ($D_2O$ solution) trans-NMA, computed with the PMM/MD procedure described here, but without the anharmonic correction, was presented in a previous paper, showing a good agreement with the experimental data [41]. The computed frequency downshift, with respect to the frequency of the isolated trans-NMA [72] (unperturbed frequency), resulted to be $56\,cm^{-1}$, reproducing most of the experimentally observed negative frequency shift $\approx$80–85 $cm^{-1}$ and in excellent agreement with the theoretical–computational estimate of 57–59 $cm^{-1}$ provided in a previous paper utilizing a method developed in the group of S. Mukamel [48]. Further, the spectrum shape and width were very well reproduced by PMM/MD calculations (fwhm $= 30\,cm^{-1}$ in both experiments and simulation). It is worth noting that the underestimation of the PMM/MD shift with respect to the experimental one is due to a combination of higher-order effects possibly including the slight inaccuracies of the calculated dipoles involved in the definition of the $\tilde{Z}_1$ matrix (see the Theory section) and the disregard of any (solute–solvent) excitonic coupling and/or intra-QC modes coupling.

Here, the amide I band is recalculated including the anharmonic correction described in the Sect. 2. In Fig. 1 are shown the vibrational spectra obtained with or without including the anharmonic correction (panel A) and the distribution of the anharmonic correction values, as obtained along the MD trajectory (panel B). The results clearly indicate that the anharmonic effect essentially provides a $16\,cm^{-1}$ frequency downshift of the whole computed spectrum. The anharmonic correction results to be virtually independent of the perturbation field, being essentially determined by the unperturbed condition (i.e. it is given by the intrinsic anharmonicity of the unperturbed energy curve). Interestingly, the anharmonic correction calculated here is comparable to the anharmonic correction estimated for the isolated trans-NMA obtained with a more sophisticated approach involving intramolecular modes coupling effects [60], and exactly reproduces the experimental estimate reported in a previous paper [48].

### 4.2 Infrared spectra in the amide I region of the GS10 peptide

The amide I band at 360 K and the unfolded–folded difference spectrum of the GS10 peptide in $D_2O$ solution, computed with the PMM/MD procedure described here, but without the anharmonic correction and the contribution

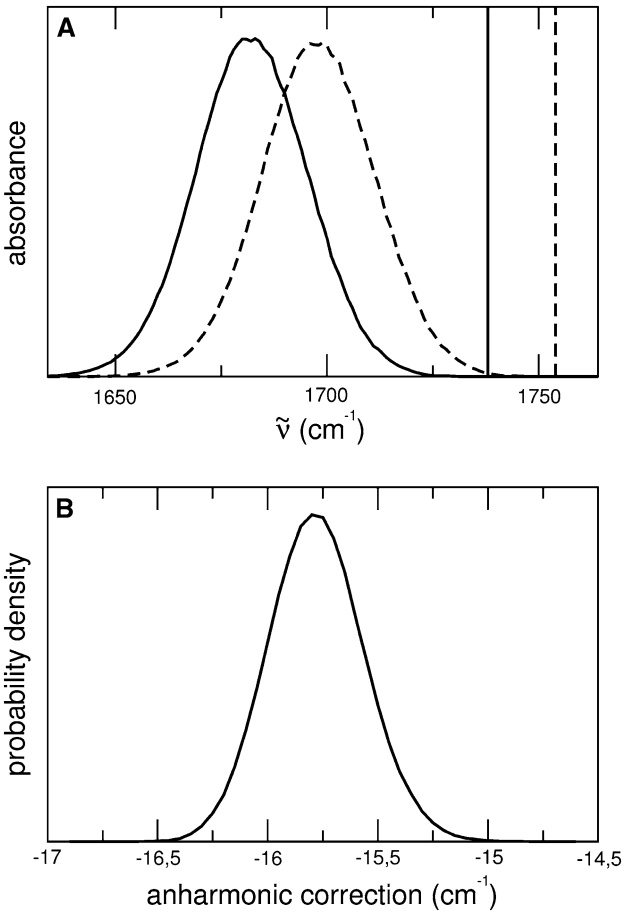


**Fig. 1** **a** Computed infrared spectrum in the amide I region of trans-NMA in $D_2O$ solution without (*dashed line*) and with (*solid line*) the anharmonic correction. The *vertical lines* indicate the unperturbed amide I frequency at the harmonic approximation (*dashed line*) and with the anharmonic correction (*solid line*). The absorbance is expressed in arbitrary units. **b** Distribution of the anharmonic corrections

of the excitonic coupling, were presented in a previous paper, showing a good agreement with the experimental data [21]. In particular, the PMM/MD calculations well reproduced the characteristic negative–positive feature of the unfolded–folded difference spectrum.

Here, the spectra are recalculated with the full procedure described in the Sect. 2, and additional data at 280 K are also presented. Similar to the case of trans-NMA (see previous subsection), also for the amide I mode of the GS10 peptide, the anharmonic correction is virtually independent of the perturbation field, being essentially given by the intrinsic anharmonicity of the unperturbed energy curve and resulting in a $16\,cm^{-1}$ frequency downshift of the whole computed spectrum (data not shown). The effect of the excitonic coupling on the amide I peak is mainly in the band shape and results in the appearance of a shoulder on the left of the main peak and in an upshift of

$\approx$15 $cm^{-1}$in the position of the peak maximum (see Fig. 2 in which the data at 280 K are reported). The shoulder, although less evident, is also present in the experimental spectrum.

In order to compare our computational results with the available experimental data [9], we present in Fig. 3 the computational and experimental spectra of the GS10 amide I band as obtained at 280 K and 360 K (the experimental data were obtained at 275 K and 358 K) together with the corresponding difference spectra. According to the analysis of the simulation data, at 280 K, GS10 can be considered as fully restricted to its folded state, while at 360 K, only the unfolded state is populated, thus confirming the assumption used in the experimental work [9]. From this figure, it is evident that the calculated spectra (with and without the use of the excitonic coupling) reproduce quite well the frequency range and the width of the experimental spectra, with a limited overestimation 10–30 $cm^{-1}$ of the position of the peak maximum. From panels A, B, and C of the same figure, it is also evident that the computed spectra properly reproduce the blue shift due to the temperature increase. Moreover, the inclusion of the excitonic coupling (panels B and E) not only reproduces the loss of Gaussian shape and the appearance of a typical shoulder in the low frequency tail, as discussed for Fig. 2, but also provides a better quantitative reproduction of the relative position of the difference spectra peaks. In fact, the inclusion of the excitonic coupling provides a shift of 19 $cm^{-1}$ versus the experimental 24 $cm^{-1}$, while the shift without the inclusion of the excitonic coupling resulted to be 33 $cm^{-1}$.

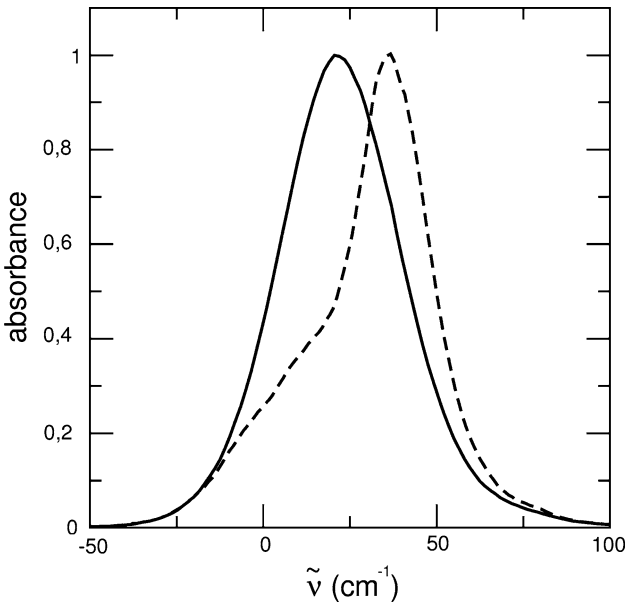


**Fig. 2** Computed equilibrium IR spectrum in the amide I region of GS10 with the inclusion of the excitonic coupling (*dashed line*) and without it (*solid line*). The spectra are calculated from the 300-ns-long simulation at 280 K described in the Sect. 3. The frequency is given as the frequency shift with respect to the frequency of the peak of trans-NMA in $D_2O$ solution. The absorbance is expressed in arbitrary units

It is also worth to note that the calculation including the excitonic coupling seems to better reproduce the intensity and asymmetry of the difference spectra signal as a result of the previously mentioned non-Gaussian shape of the spectra. However, the computed difference spectra (panels D and E) fail to reproduce the experimental splitting of the positive peak (panel F). The reason of this discrepancy is currently under investigation.

## 5 Conclusions

In this paper, we present an extension of a previously reported PMM/MD-based procedure to model IR spectra of polyatomic chemical systems in condensed phase. The present methodology, which includes in the model the anharmonic correction and excitonic coupling, provides a physically coherent theoretical–computational method to model IR spectra of polyatomic systems embedded into a complex atomic-molecular environment.

The use of the PMM framework to reconstruct the quantum vibrational states allows the direct modeling of the excitation process, explicitly treating the perturbation effect due to the fluctuating environment without involving any empirical term and/or adjustable parameter. Application of the method to reproduce the complex folding–unfolding IR signal variations of the amide I band of a $\beta$-hairpin peptide shows the quantitative accuracy of the approach employed and its potential to model IR signals of macromolecules in solution, both in their folded and in unfolded state.

The main feature of the method is that the IR behavior can be accurately reproduced also for very heterogeneous states, such as peptide and protein unfolded states, whose IR spectrum is commonly difficult to be computed due to their conformational high flexibility. Interestingly, the inclusion of the excitonic coupling although providing limited effects on the spectral signal seems to be important to properly reproduce some spectral details.

Finally, it is worth to note that the present implementation of the method, based on assuming weak anharmonicity and no relevant modes coupling beyond excitonic interactions for the ground and first excited vibrational states, might be inefficient to treat systems where perturbation effects result in a significant intramolecular or even intermolecular mixing of vibrational modes. For such conditions (e.g. the stretching modes of liquid water), our PMM/MD approach might be still usable although

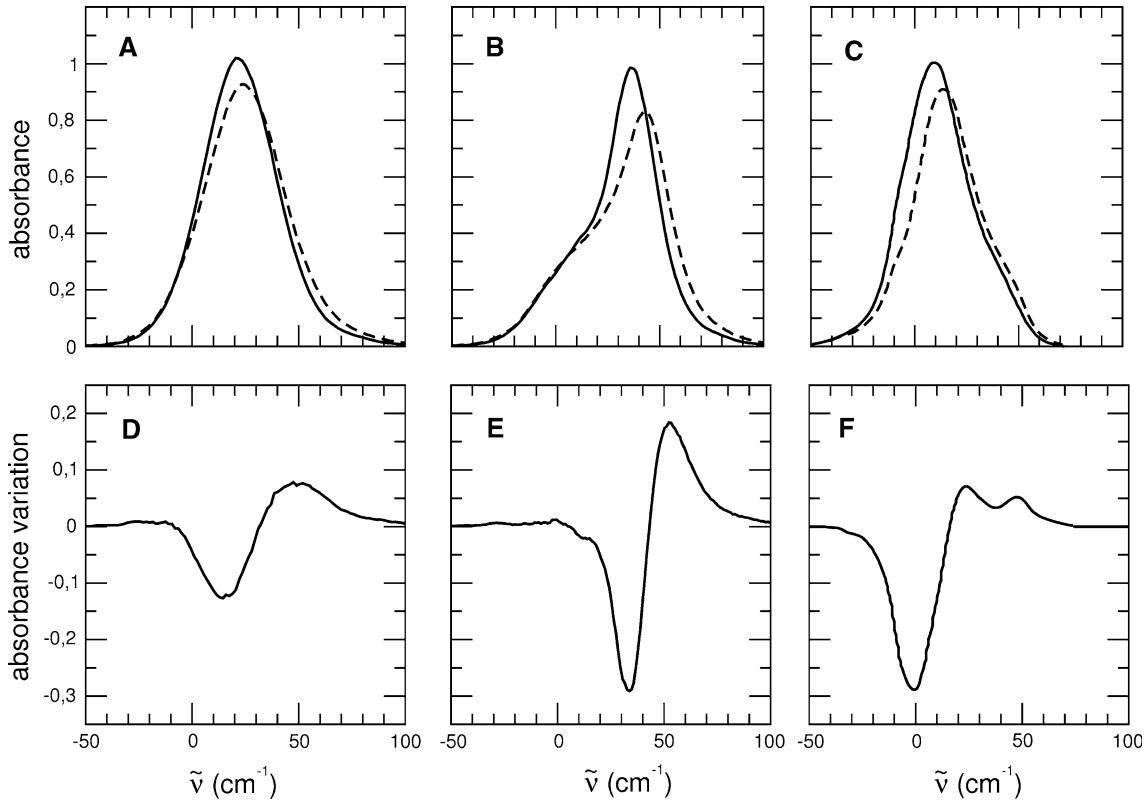


**Fig. 3** Computed IR spectra in the amide I region of GS10 without the inclusion of the excitonic coupling (**a**) and with the inclusion of the excitonic coupling (**b**) as obtained from the MD simulations at 280 K (*solid line*) and at 360 K (*dashed line*). The two temperatures virtually correspond respectively to the folded and unfolded states. **c** Experimental spectra at 275 K (*solid line*) and 358 K (*dashed line*). Computed difference spectra generated by subtracting the spectrum at 280 K from the spectrum at 360 K without (**d**) and with (**e**) the inclusion of the excitonic coupling. **f** Experimental difference spectra generated by subtracting the spectrum at 275 K from the spectrum at 358 K. To provide an easier comparison of the computed and experimental spectra, the intensities of the lower temperature spectra have been all normalized to 1. This makes the intensities of the difference spectra directly comparable. The frequency is given as the frequency shift with respect to the frequency of the peak of trans-NMA in $D_2O$ solution ($1,682\,\mathrm{cm}^{-1}$ from our calculations and $1,622\,\mathrm{cm}^{-1}$ from experimental data)

requiring a more complex and computationally inefficient implementation as briefly mentioned in the Sect. 2. However, the test cases presented in this paper clearly show that, even when chromophore–solvent and chromophore–chromophore hydrogen-bonding interactions are present, if the solvent and chromophore modes are characterized by not overlapping frequencies, the invariant mode approximation combined with the excitonic coupling furnishes a rather accurate model providing the essential quantitative features of the spectral signal.

**Acknowledgments** This work was supported by the Italian FIRB RBIN04PWNC_001 "Structure, function, dynamics and folding of proteins" founded by MIUR. We also acknowledge the University of Rome "La Sapienza" for financial support with the project "MORFOGENESI MOLECOLARE: un approccio multidisciplinare per lo studio del folding e misfolding delle proteine" and CASPUR (Consorzio interuniversitario per le Applicazioni di Supercalcolo Per Universitá e Ricerca) for the use of its computational facilities and the use of Gaussian.

## Appendix 1

In this appendix, we schematize the computational procedure employed to obtain the amide I vibrational spectrum of a solvated peptide and/or protein. Note that the method may be straightforwardly generalized for any vibrational mode (e.g. the amide II mode).

1. In the first steps, the model describing each unperturbed oscillator (i.e. each peptide group along the peptide/protein backbone) is constructed (trans-NMA is used as the model system of the peptide group):
   - Calculation of the mass-weighted Hessian for the unperturbed (isolated) trans-NMA;
   - Selection of the eigenvector associated with the amide I mode providing the selected mode coordinate;

- Generation of a number of configurations of the isolated trans-NMA along the selected mode coordinate;
- Quantum chemical calculations in order to obtain for each of the above-mentioned configurations a selected number of unperturbed electronic states, and the corresponding eigenvalues and dipole operator elements, which provide the basis to construct the electronic Hamiltonian matrix (see Eqs. 14 and 15). Note that for this purpose, a computational method able to provide a set of orthonormal unperturbed electronic states is necessary (e.g. state averaged complete active space, linear response theory-based calculations, etc.).

2. In the next steps, the perturbed electronic ground-state energy along the selected mode coordinate is calculated for each peptide group of the solvated peptide/protein at each MD frame of an extended MD simulation of the peptide/protein embedded into the solvent molecules as follows:

- Construction of the perturbed electronic Hamiltonian matrix (see Eqs. 14 and 15) after having fitted trans-NMA (i.e. each electric dipole moment of trans-NMA) on the given peptide group. Note that the perturbing field (Eqs. 14 and 15) is exerted by the solvent molecules, the rest of the peptide/protein molecular framework and the side chain of the selected residue;
- Evaluation of the ground-state perturbed electronic energy by diagonalization of the perturbed electronic Hamiltonian;
- Repeating of the two previous steps for each configuration along the mode coordinate (i.e. using the unperturbed energies and electric dipoles of each configuration) to evaluate the perturbed electronic energies along the selected mode coordinate;
- Numerical fit of the perturbed energy curve obtained in the previous step providing the perturbed harmonic frequencies and anharmonic corrections (Eq. 12 and 13).

3. The perturbed frequencies for each oscillator along the peptide/protein system at each MD frame are finally used to include the excitonic effects as follows:

- Construction and diagonalization of the excitonic matrix (see Eqs. 20–27) providing the set of eigenvalues and eigenvectors to be used to calculate the transition dipoles for each excitonic excitation (Eq. 27). Note that the elements of such a matrix are obtained by using only the perturbed electronic ground states of each peptide group;
- Calculation of the vibrational spectrum of the whole peptide/protein embedded into the solvent via the application of Eq. 28 over the whole MD trajectory.

## Appendix 2

Defining with $\boldsymbol{r}_n$ and $\boldsymbol{p}_n$ the Cartesian nuclear coordinates and conjugated momenta, we can express the nuclear kinetic energy operator as

$$\hat{K} = \hat{\boldsymbol{p}}_n^T \frac{\tilde{M}_{r_n}^{-1}}{2} \hat{\boldsymbol{p}}_n \tag{29}$$

$$\hat{p}_j = -i\hbar \frac{\partial}{\partial r_{n,j}} \tag{30}$$

where $\tilde{M}_{r_n}^{-1}$ is the inverse of the usual diagonal mass tensor. From the definition of the conjugated momenta operators, we can easily obtain the momenta operator transformation ($\hat{\boldsymbol{p}}_n \rightarrow \hat{\boldsymbol{\pi}}_n$) associated with the coordinates transformation ($\boldsymbol{r}_n \rightarrow \boldsymbol{\eta}_n$)

$$\hat{\pi}_{n,j'} = -i\hbar \sum_j \left( \frac{\partial r_{n,j}}{\partial \eta_{n,j'}} \right) \frac{\partial}{\partial r_{n,j}} \tag{31}$$

or in vector notation

$$\hat{\boldsymbol{\pi}}_n = \tilde{T}^T \hat{\boldsymbol{p}}_n \tag{32}$$

$$T_{j,j'} = \left( \frac{\partial r_{n,j}}{\partial \eta_{n,j'}} \right) \tag{33}$$

Hence, the kinetic energy operator becomes

$$\hat{K} = \hat{\boldsymbol{\pi}}_n^T \frac{\tilde{M}_{\eta_n}^{-1}}{2} \hat{\boldsymbol{\pi}}_n \tag{34}$$

$$\tilde{M}_{\eta_n}^{-1} = \tilde{T}^{-1} \tilde{M}_{r_n}^{-1} \left[ \tilde{T}^{-1} \right]^T \tag{35}$$

which is completely equivalent to the classical expression, although it is to be considered that dealing with operators (i.e. $\hat{p}_j T_{j,j'} \neq T_{j,j'} \hat{p}_j$) we have

$$(\hat{\boldsymbol{p}}_n^T)_j = (\hat{\boldsymbol{p}}_n)_j = -i\hbar \frac{\partial}{\partial r_{n,j}} \tag{36}$$

$$(\hat{\boldsymbol{\pi}}_n^T)_{j'} = \sum_j \hat{p}_j T_{j,j'} = -i\hbar \sum_j \frac{\partial T_{j,j'}}{\partial r_{n,j}} - i\hbar \frac{\partial}{\partial \eta_{n,j'}} \tag{37}$$

$$(\hat{\boldsymbol{\pi}}_n)_{j'} = \sum_j T_{j,j'} \hat{p}_j = -i\hbar \frac{\partial}{\partial \eta_{n,j'}} \tag{38}$$

For a rigid QC with quantum internal Cartesian coordinates ($\boldsymbol{\beta}$) and classical rototranslational ones ($\boldsymbol{\xi}'$), we may write [40, 49, 50]

$$\tilde{M}_{\eta_n}^{-1} = \begin{pmatrix} \tilde{D}_{\xi,\xi} & \tilde{D}_{\xi,\beta} \\ \tilde{D}_{\beta,\xi} & \tilde{D}_{\beta,\beta} \end{pmatrix} \cong \begin{pmatrix} \tilde{D}_{\xi,\xi} & \tilde{0} \\ \tilde{0} & \tilde{D}_{\beta,\beta} \end{pmatrix} \tag{39}$$

providing

$$\hat{K} \cong \hat{K}_{\xi} + \hat{K}_{\beta} \tag{40}$$

$$2\hat{K}_{\xi} = \hat{\boldsymbol{\pi}}_{\xi}^{T} \tilde{D}_{\xi,\xi} \hat{\boldsymbol{\pi}}_{\xi} \tag{41}$$

$$2\hat{K}_{\beta} = \hat{\boldsymbol{\pi}}_{\beta}^{T} \tilde{D}_{\beta,\beta} \hat{\boldsymbol{\pi}}_{\beta} \tag{42}$$

where both $\tilde{D}_{\xi,\xi}$ and $\tilde{D}_{\beta,\beta}$ can be considered as independent of the internal Cartesian coordinates, i.e. the $\boldsymbol{\beta}$ coordinates are "classically" virtually fixed at $\boldsymbol{\beta} = \boldsymbol{\beta}_0$.

Finally, it is worth to note that in our approach, we distinguish between classical and quantum nuclear degrees of freedom approximating the Hamiltonian eigenstates, for a single QC, as the product of an electronic eigenfunction $\Phi(\boldsymbol{x}, \boldsymbol{\xi}', \boldsymbol{\beta})$ with two nuclear wave functions, $\phi_v(\boldsymbol{\beta})$ and $\phi_{\xi,\pi_\xi}(\boldsymbol{\xi}')$ describing the quantum vibrational and classical nuclear degrees of freedom, respectively. In the previous wave functions $\boldsymbol{x}$ are the (Cartesian) electronic coordinates, $\boldsymbol{\xi}', \boldsymbol{\beta}$ the nuclear classical and quantum coordinates respectively and $\phi_{\xi,\pi_\xi}$ is fully confined within a phase space differential volume and so it acts transforming the classical nuclear coordinates and conjugated momenta operators into the phase space values $\boldsymbol{\xi}, \boldsymbol{\pi}_\xi$, i.e. it is a wave packet in $\boldsymbol{\xi}, \boldsymbol{\pi}_\xi$ space. Therefore, for any observable expressed by the operator $\hat{O}$ and introducing the Jacobean $J(\boldsymbol{\xi}', \boldsymbol{\beta})$ for the $\boldsymbol{r}_n \rightarrow \boldsymbol{\xi}', \boldsymbol{\beta}$ transformation, we have

$$\begin{aligned} &< \phi_{v,i,i'} \phi_{\xi,\pi} \Phi_i | \hat{O} | \Phi_l \phi_{\xi_\xi} \phi_{v,l,l'} > \\ &= \int \phi^*_{v,i,i'}(\boldsymbol{\beta}) \phi^*_{\xi,\pi_\xi}(\boldsymbol{\xi}') \Phi^*_i(\boldsymbol{x}, \boldsymbol{\xi}', \boldsymbol{\beta}) \hat{O} \Phi_l(\boldsymbol{x}, \boldsymbol{\xi}', \boldsymbol{\beta}) \\ &\quad \phi_{v,l,l'}(\boldsymbol{\beta}) \phi_{\xi,\pi_\xi}(\boldsymbol{\xi}') J(\boldsymbol{\xi}', \boldsymbol{\beta}) \mathrm{d}\boldsymbol{\xi}' \mathrm{d}\boldsymbol{\beta} \mathrm{d}\boldsymbol{x} \\ &= \int \phi^*_{v,i,i'}(\boldsymbol{\beta}) \Phi^*_i(\boldsymbol{x}, \boldsymbol{\xi}, \boldsymbol{\beta}) \hat{O} \Phi_l(\boldsymbol{x}, \boldsymbol{\xi}, \boldsymbol{\beta}) \phi_{v,l,l'}(\boldsymbol{\beta}) J(\boldsymbol{\xi}, \boldsymbol{\beta}) \mathrm{d}\boldsymbol{\beta} \mathrm{d}\boldsymbol{x} \\ &\cong J(\boldsymbol{\xi}, \boldsymbol{\beta}_0) \int \phi^*_{v,i,i'}(\boldsymbol{\beta}) \Phi^*_i(\boldsymbol{x}, \boldsymbol{\xi}, \boldsymbol{\beta})^* \hat{O} \Phi_l(\boldsymbol{x}, \boldsymbol{\xi}, \boldsymbol{\beta}) \phi_{v,l,l'}(\boldsymbol{\beta}) \mathrm{d}\boldsymbol{\beta} \mathrm{d}\boldsymbol{x} \end{aligned} \tag{43}$$

where the double index of $\phi_v$ provides the electronic and vibrational states defining the vibrational wave function and typically $J(\boldsymbol{\xi}, \boldsymbol{\beta}_0)$ is omitted [40] including $\sqrt{J(\boldsymbol{\xi}, \boldsymbol{\beta}_0)}$ in $\phi_v$, i.e. the vibrational eigenstates are renormalized.

## References


1. Slayton RM, Anfirud PA (1997) Curr Opin Struct Biol 7:717
2. Zanni MT, Hochstrasser RM (2001) Curr Opin Struct Biol 11:516
3. Kim S, Lim M (2005) J Am Chem Soc 127:5786
4. Nienhaus K, Olson JS, Franzen S, Nienhaus GU (2005) J Am Chem Soc 127:40
5. Bredenbeck J, Helbing J, Kumita JR, Woolley GA, Hamm P (2005) Proc Natl Acad Sci USA 102:2379
6. Huang C, Getahun Z, Zhu Y, Klemke J, DeGrado W, Gai F (2002) Proc Natl Acad Sci USA 99:2788
7. Ihalainen JA, Bredenbeck J, Pfister R, Helbing J, Chi L, van Stokkum IH, Woolley GA, Hamm P (2007) Proc Natl Acad Sci USA 104:5383
8. Kolano C, Helbing J, Kozinski M, Sander W, Hamm P (2006) Nat Biotechnol 444:469
9. Maness SJ, Franzena S, Gibbs AC, Causgrove TP, Dyer RB (2003) Biophys J 84:3874
10. Smith AW, Tokmakoff A (2007) Angew Chem Int Ed Engl 46:7984
11. Xu Y, Oyola R, Gai F (2003) J Am Chem Soc 125:15388
12. Gaigeot MP, Vuilleumier R, Sprik M, Borgis D (2005) J Chem Theory Comput 1:772
13. Gorbunov RD, Nguyen PH, Kobus M, Stock G (2007) J Chem Phys 126:054509
14. Nutt DR, Meuwly M (2007) ChemPhysChem 8:527
15. Yang S, Cho M (2005) J Chem Phys 123:134503
16. Yang S, Cho M (2009) J Chem Phys 131:135102
17. Klahn M, Schlitter J, Gerwert K (2005) Biophys J 88:3829
18. Corcelli SA, Skinner JL (2005) J Phys Chem A 109:6154
19. Kwac K, Cho M (2003) J Chem Phys 119:2247
20. Schmidt JR, Corcelli SA, Skinner JL (2004) J Chem Phys 121:8887
21. Amadei A, Daidone I, Di Nola A, Aschi M (2010) Curr Opin Struct Biol 20:155
22. Bour P, Keiderling TA (2005) J Phys Chem B 109:23687
23. Brauner JW, Flach CR, Mendelsohn R (2005) J Am Chem Soc 127:100
24. Choi JH, Lee H, Lee KK, Hahn S, Cho M (2007) J Chem Phys 126:045102
25. Hahn S, Ham S, Cho M (2005) J Phys Chem B 109:11789
26. Ham S, Cha S, Choi JH, Cho M (2003) J Chem Phys 119:1451
27. Krimm S, Bandekar J (1986) Adv Protein Chem 38:181
28. Lee SH, Krimm S (1998) Biopolymers 46:283
29. Moran A, Mukamel S (2004) Proc Natl Acad Sci USA 101:506
30. Smith AW, Tokmakoff A (2007) J Chem Phys 126:045109
31. Torii H, Tasumi M (1992) J Chem Phys 96:3379
32. Calvo F, Parneix P, Van-Oanh NT (2010) J Chem Phys 132:124308
33. Huang X, Habershon S, Bowman JM (2008) Chem Phys Lett 450:253
34. Kaczmarek A, Shiga M, Marx D (2009) J Phys Chem A 113(10):1985
35. Pavese M, Berard DR, Voth GA (1999) Chem Phys Lett 300:93
36. Schmitz M, Tavan P (2004) J Chem Phys 121:12233
37. Witt A, Ivanov SD, Shiga M, Forbert H, Marx D (2009) J Chem Phys 130:194510
38. Barth A, Zscherp C (2002) Q Rev Biophys 35:369
39. Hayashi T, Mukamel S (2007) J Phys Chem B 111:11032
40. Amadei A, Marinelli F, D'Abramo M, D'Alessandro M, Anselmi M, Di Nola A, Aschi M (2005) J Chem Phys 122:124506
41. Daidone I, Aschi M, Zanetti-Polzi L, Nola AD, Amadei A (2010) Chem Phys Lett 488:213
42. Amadei A, D'Abramo M, Zazza C, Aschi M (2003) Chem Phys Lett 381:187
43. Amadei A, D'Alessandro M, D'Abramo M, Aschi M (2009) J Chem Phys 130:08410
44. Aschi M, Spezia R, Di Nola A, Amadei A (2001) Chem Phys Lett 344:374
45. Spezia R, Aschi M, Di Nola A, Amadei A (2002) Chem Phys Lett 365:450
46. Anselmi M, Aschi M, Di Nola A, Amadei A (2007) Biophys J 92:3442

47. Hayashi T, la Cour Jansen T, Zhuang W, Mukamel S (2005) J Phys Chem A 109:64
48. Hayashi T, Zhuang W, Mukamel S (2005) J Phys Chem A 109:9747–9759
49. Amadei A, Chillemi G, Ceruso MA, Grottesi A, Di Nola A (2000) J Chem Phys 112:9
50. Gallavotti G (1983) The elements of mechanics. Springer, New York
51. Dirac PAM (1958) The principles of quantum mechanics. Clarendon, Oxford
52. Cappelli C, Monti S, Scalmani G, Barone V (2010) J Chem Theory Comput 6:1660
53. Danecek P, Bour P (2006) J Comput Chem 28:1617
54. Dunn ME, Evans TM, Kirschner KN, Shields GH (2006) J Phys Chem A 110:303
55. Gerber RB, Brauer R, Gregurick S, Chaban GM (2002) Phys Chem Comm 21:142
56. Hrenar T, Werner HJ, Rauhut G (2007) J Chem Phys 126:134108
57. Yu X, Leitner DM (2003) J Phys Chem B 107:1698
58. Leitner DM (2008) Ann Rev Phys Chem 59:233
59. Nguyen PH, Park SM, Stock G (2010) J Chem Phys 132:025102
60. Gregurick SK, Chaban GM, Gerber RB (2002) J Phys Chem A 106:8696
61. Atkins PW, Friedman RS (1997) Molecular quantum mechanics. Oxford University Press, New York
62. Frisch MJ et al (2004) Gaussian 03, Revision C.02. Gaussian Inc, Wallingford
63. van der Spoel D, van Drunen R, Berendsen HJC (1994) Groningen machine for chemical simulation. Department of Biophysical Chemistry, BIOSON Research Institute, Nijenborgh 4 NL-9717 AG Groningen
64. van Gunsteren WF, Billeter SR, Eising AA, Hünenberger PH, Krüger P, Mark AE, Scott WRP, Tironi IG (1996) Biomolecular simulation: the GROMOS96 manual and user guide. Hochschulverlag AG an der ETH Zürich, Zürich
65. Besler BH, Merz KM Jr, Kollman PA (1990) J Comput Chem 11:431
66. Berendsen HJC, Postma JPM, van Gunsteren WF, Hermans J (1981) In: Pullman B (ed) Intermolecular forces. D. Reidel Publishing Company, Dordrecht, pp 331–342
67. Hess B, Bekker H, Berendsen HJC, Fraaije JGEM (1997) J Comput Chem 18:1463
68. Darden T, York D, Pedersen L (1993) J Chem Phys 98:10089
69. Evans DJ, Morriss GP (1990) Statistical mechanics of nonequilibrium liquids. Academic Press, London
70. Gibbs AC, Kondejewski LH, Gronwald W, Nip A, Hodges R, Sykes BD, Wishart DS (1998) Nat Struct Biol 5:284
71. Berendsen HJC, Grigera JR, Straatsma TP (1987) J Phys Chem 91:6269
72. Kubelka J, Keiderling TA (2001) J Phys Chem A 105:10922